ENGINEERING

Algorithmic encoding of adaptive responses in temperature-sensing multimaterial architectures

Weichen Li^{1†}, Yue Wang^{2†}, Tian Chen^{2*}, Xiaojia Shelly Zhang^{1,3,4}*

We envision programmable matters that can alter their physical properties in desirable manners based on user input or autonomous sensing. This vision motivates the pursuit of mechanical metamaterials that interact with the environment in a programmable fashion. However, this has not been systematically achieved for soft metamaterials because of the highly nonlinear deformation and underdevelopment of rational design strategies. Here, we use computational morphogenesis and multimaterial polymer 3D printing to systematically create soft metamaterials with arbitrarily programmable temperature-switchable nonlinear mechanical responses under large deformations. This is made possible by harnessing the distinct glass transition temperatures of different polymers, which, when optimally synthesized, produce local and giant stiffness changes in a controllable manner. Featuring complex geometries, the generated structures and metamaterials exhibit fundamentally different yet programmable nonlinear force-displacement relations and deformation patterns as temperature varies. The rational design and fabrication establish an objective-oriented synthesis of metamaterials with freely tunable thermally adaptive behaviors. This imbues structures and materials with environmentaware intelligence.

Copyright © 2023 The Authors, some rights reserved; exclusive licensee American Association for the Advancement of Science. No claim to original U.S. Government Works. Distributed under a Creative Commons Attribution NonCommercial License 4.0 (CC BY-NC).

INTRODUCTION

Programmable matters alter their physical properties in response to user or environmental input in a designable fashion (1). This motivates the development of mechanical metamaterials with exotic behaviors (2-5), yet most behaviors remain unchangeable throughout their lifetime, as they are not designed to interact with the environment, such as temperature. Hence, a recent focus is to develop metamaterials with mechanical responses adapting to or interacting with the ambient environment, such as temperature (6-8), magnetic field (9-13), electric voltage (14), air pressure (15), and the presence of water (16), and many of these metamaterials can be four dimensionally (4D) printed (17).

This study focuses on mechanical metamaterials with temperature-switchable functional changes under large deformations realized in a fully programmable fashion. We aim to establish and harness a one-to-one mapping between temperature and nonlinear mechanical behavior through the metamaterial. In the literature, a widely adopted approach to achieve temperature-dependent behaviors is using shape memory materials that actuate and alter mechanical behaviors (18–25), such as deformation modes (20) and effective properties (19). However, the accompanied shape changes in the unloaded states may not suit applications requiring functional changes, such as force-displacement (FD) responses dissociated from shape changes and free of external power or intervention.

To achieve a fully automatic temperature-induced behavioral change, an effective strategy is to use composites made of polymeric materials with disparate glass transition temperatures to realize temperature-induced local stiffness changes for the manipulation of global mechanical responses. Examples include temperature-tunable bistability (26), metamaterial anisotropy and Poisson's ratio (6), bandgaps (27), and self-recoverable deployment (7). However, existing metamaterials of this type are largely designed in a forward fashion, which could achieve a certain class of target responses produced by relatively regular design patterns but have limited freedom in achieving complex behaviors at will. Accurately attaining arbitrarily prescribed nonlinear and large-deformation behaviors may only be achieved by structures featuring intricate geometry and material distributions, which could be systematically obtainable through computational morphogenesis approaches such as optimization (5, 28) and artificial intelligence (29).

As a computational morphogenesis technique, topology optimization (30, 31) has demonstrated great success in producing metamaterials with complex programmed behaviors such as programmable Poisson's ratios (2) and nonlinear mechanical responses (5, 28). Topology optimization has also been used for achieving environmentally interactive behaviors, such as temperature-dependent bandgaps (32). However, most topology optimization-based designs of environmentally adaptive responses assume the linear setup that could not capture or harness the rich nonlinear behaviors desired for various applications made of soft materials or undergo large deformations. In addition, the peculiar properties of most topology optimization-designed metamaterials are numerical and short of experimental validation. Hence, a large gap persists in the free-form inverse design capacity of highly nonlinear and environmentally interactive behaviors, as well as in the physical realization of the programmed exotic responses.

In this study, we inversely design, fabricate, and validate a class of polymeric metamaterials that exhibit precisely and arbitrarily programmable environment-adaptive nonlinear mechanical behaviors under different temperatures. We aim to realize thermally switchable nonlinear FD relations and deformation modes under large deformations by exploiting the different glass transition temperatures

¹Department of Civil and Environmental Engineering, University of Illinois Urbana-Champaign, Urbana, IL 61801, USA. ²Department of Mechanical Engineering, University of Houston, Houston, TX 77204, USA. ³Department of Mechanical Science and Engineering, University of Illinois Urbana-Champaign, Urbana, IL 61801, USA.

⁴National Center for Supercomputing Applications, Urbana, IL 61801, USA. *Corresponding author. Email: zhangxs@illinois.edu (X.S.Z.); tianchen@central.uh. edu (T.C.)

[†]These authors contributed equally to this work.

and stiffness of two 3D-printable polymers through the fully automated and experience-free multimaterial topology optimization—based generative algorithm. The generated designs feature irregular geometries and material phase distributions, and they are fabricated using multimaterial 3D printing. The experiments validate the accurate realization of various prescribed dissimilar nonlinear FD responses and deformation patterns under two designated temperatures. Our proposed inverse design framework can be generalized to programming metamaterial's interactions with other physics, such as electromagnetic fields, humidity, and light. We envision that the design and fabrication strategy will effectively advance the creation and application of environmentally switchable nonlinear behaviors in smart materials, soft robotics, and sensors.

RESULTS

We use polymers FLX9895 (FLX) and ElasticoBlack (EB) for the composites. They are printed simultaneously by the Stratasys J35 Pro 3D Printer with a polar coordinate system (see figs. S1 and S2 for details). The two polymers have distinct glass transition temperatures T_g and overall stiffness as illustrated in Fig. 1A (see sections

S1.2.2 and S1.3 for details). At 10°C, the initial stiffness of FLX is approximately 60 times larger than that of EB, whereas at 60°C (higher than the T_g of both materials), FLX is about 4 times larger. The large contrast in stiffness produces a spatially nonuniform change in the overall response of the synthesized composites. This forms the basic physical mechanism for realizing dissimilar nonlinear behaviors under different temperatures other than a homogeneous stiffness change. Such a mechanism is unavailable from a single-material structure. At a microscopic scale, FLX is a digital material created at the time of printing using EB as the base material and VeroUltraWhite as the inclusion (33). This contributed to the well-bonded interfaces between FLX and EB during fabrication, as both share the same base material. During testing, these interfaces did not exhibit failure under both temperatures. The behavior is in accordance with the findings of Mueller et al. (34), who studied multimaterial interfaces on the micrometer scale with a 3D printer using the same PolyJet technology. Both materials are viscoelastic, and their quasi-static behaviors are modeled as nonlinear hyperelastic materials. The stress-stretch curves of the two materials at 10° and 60°C are given in fig. S5 and fitted using a two-term Ogden model (35, 36), which will be input into the numerical

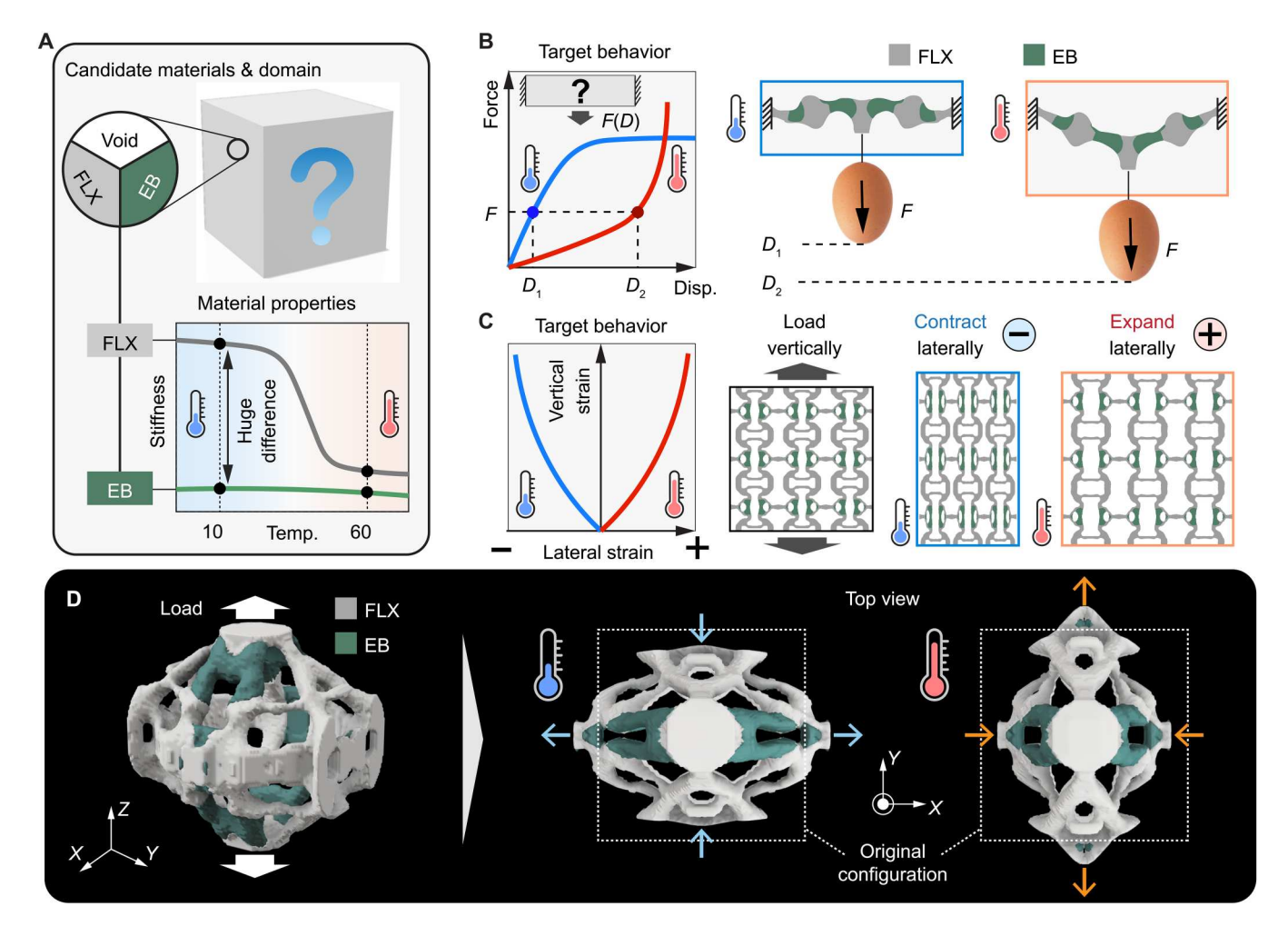


Fig. 1. Programming adaptive nonlinear mechanical responses for different temperatures. (A) Design domain and candidate polymeric materials with temperature-dependent stiffness. (B) Disparate target structural FD responses under two different temperatures. (C) Disparate nonlinear temperature-dependent deformation modes for 2D metamaterial and (D) for 3D structures. See movie S1 for the design, fabrication, and testing pipeline.

simulation and inverse design. Details of the materials and modeling are provided in section S1.

The key to programming adaptive temperature-dependent nonlinear behaviors lies in the strategic design of the geometry and material distribution. To achieve this, we use multimaterial topology optimization, which is widely used to generate metamaterials with programmed properties (2, 5, 28, 37–39). Multimaterial topology optimization requires density and material design variables to define the geometry and material phase distributions of a composite structure, respectively. The design variables are associated with the material's properties (in this case, the hyperelastic stored-energy density functions of the two polymers) through interpolation schemes. On the basis of these setups, we formulate the inverse design optimization problem as follows: Vary the geometry and material phase distributions to minimize the error between the composite's actual behavior predicted by nonlinear finite element analysis (FEA) and the prescribed target behavior. The optimization problem includes functional constraints to prevent designs with premature failure and excessive deformation. The constrained optimization problem is solved by the method of moving asymptotes (40). Details of the multilateral design, FEA, and optimization formulation are provided in section S3.

Programming temperature-switchable nonlinear mechanical responses

We first focus on realizing disparate temperature-switchable nonlinear FD responses at 10° and 60°C. Nonlinear FD curves, such as those with buckling and force plateaus, are desired for applications such as impact absorption (41) and vibration isolation devices (42). For the inverse design, we use the design domain shown in Fig. 2A, where the structure is fixed on two sides and loaded at the top through prescribed displacement to produce the two sets of target FD curves illustrated in Fig. 2, C and D. The two target curves (within each set) with fundamentally different features are prescribed through a number of control points on the FD plot. Details of the optimization formulation and solution procedure are provided in sections S3.4.1 and S3.5, respectively. Target 1 shows buckling behavior at 10°C and stiffening behavior at 60°C, and target 2 is a trilinear relation at 10°C and a rapid stiffening at 60°C.

For target 1, the optimization-generated design and 3D-printed specimen are shown in Fig. 2C, and the specimen is tested using a universal testing machine (Instron 5969S2126) with a mounted chamber for temperature control (Fig. 2B). The experiment and simulation nonlinear FD curves under the two temperatures achieve the prescribed targets (Fig. 2E). The structure has two upper and two lower branches attaching to the sides and forming two openings, with the FLX occupying mainly the top half and EB at the bottom half. At 10°C, as EB's contribution is small, the behavior is dominated by the FLX at the top, which has the features of a buckling beam structure. Hence, the buckling of the two slender arms results in a sudden drop in the stiffness and the large rotation of the two arms. At 60°C, both materials contribute, and the overall geometry dominates the behavior. In the beginning, because of the temperature-induced softening, the structural stiffness was relatively low, but subsequent loading stretched the originally curved EB members into straight bars and switched its deformation from bending-dominated to stretch-dominated, resulting in the stiffening FD response.

Inverse design with target FD 2 produces the composite structure shown in Fig. 2D. Both materials appear in the design, with FLX appearing at the two ends and part of the two horizontal members while the EB is occupying the center and part of the two members. The stiff FLX forms thin joints at the two sides, which are typical features for buckling structures. At 10°C, FLX dominates but EB also contributes because of its large proportion, and the buckling of FLX members produces the softening and the following plateau stage. The large rotation deforms the two arms into straighter members and revives the high stiffness at the following loading stage. At 60°C, as FLX considerably softens, its buckling effect is diminished, and both materials contribute. The structure's behavior is controlled by the collective geometry of two thick members initially curved and subsequently straightened. This produces the rapidly stiffening FD responses (Fig. 2F).

The target FD 1 in Fig. 2E shows some discrepancies between the experimental and simulation curves. The discrepancy could be attributed to geometric defects from the fabrication of the thin FLX members near the loading region and the side supports. This discrepancy is present only in the 10°C case, where FLX dominates, and is absent for the structure in Fig. 2F, with larger member size and under tension loading. At 10°C, the structure's behavior is mainly determined by the FLX regions because of their dominating stiffness, and their small size indicates a high sensitivity to geometric defects. Furthermore, the defect's impact can be magnified by the buckling under compression loading, as buckling is sensitive to geometric variations. A third potential factor exacerbating the fitting may be the relatively high viscosity of FLX and EB at 10°C, which is not directly considered in our simulation and optimization. Although the structure is loaded at a low rate, viscous behavior may have a local influence due to the nonuniform strain rate in the structure. A detailed comparison under different loading rates is provided in section S2.1.1. A systematic investigation of these factors presents a meaningful next step.

To visually demonstrate extremely large yet programmable changes in stiffness, we show the deformed shapes of target 2 structure when subjected to an equal weight of an egg (0.68 N) under both 10° and 60°C (Fig. 2G). The displacement at 10°C at D_1 is much smaller than the displacement D_2 at 60°C. These measured displacements match the target FD curves at a force equaling the egg's weight, thereby demonstrating the validity of the algorithm (rightmost plot of Fig. 2G).

Temperature-switchable nonlinear deformation modes for metamaterial

Next, we program temperature-controlled deformation patterns in 2D periodic metamaterials by optimizing the microstructure of the unit cells. Specifically, we demonstrate dissimilar target nonlinear lateral deformations at two designated temperatures when the metamaterial is subjected to the same vertical displacement.

Assuming periodic response and the absence of symmetry breaking, the optimization focuses on one unit cell subjected to 20% average applied vertical strain and a periodic boundary condition. The design variables are the geometry and material phases of the unit cell structure, which are characterized by the density and material design variables, respectively (see sections S3.1 and S3.2 for details). The objective is to minimize the errors between the actual average lateral strain predicted by the FEA and the prescribed target lateral strain under two different temperatures. To ensure the

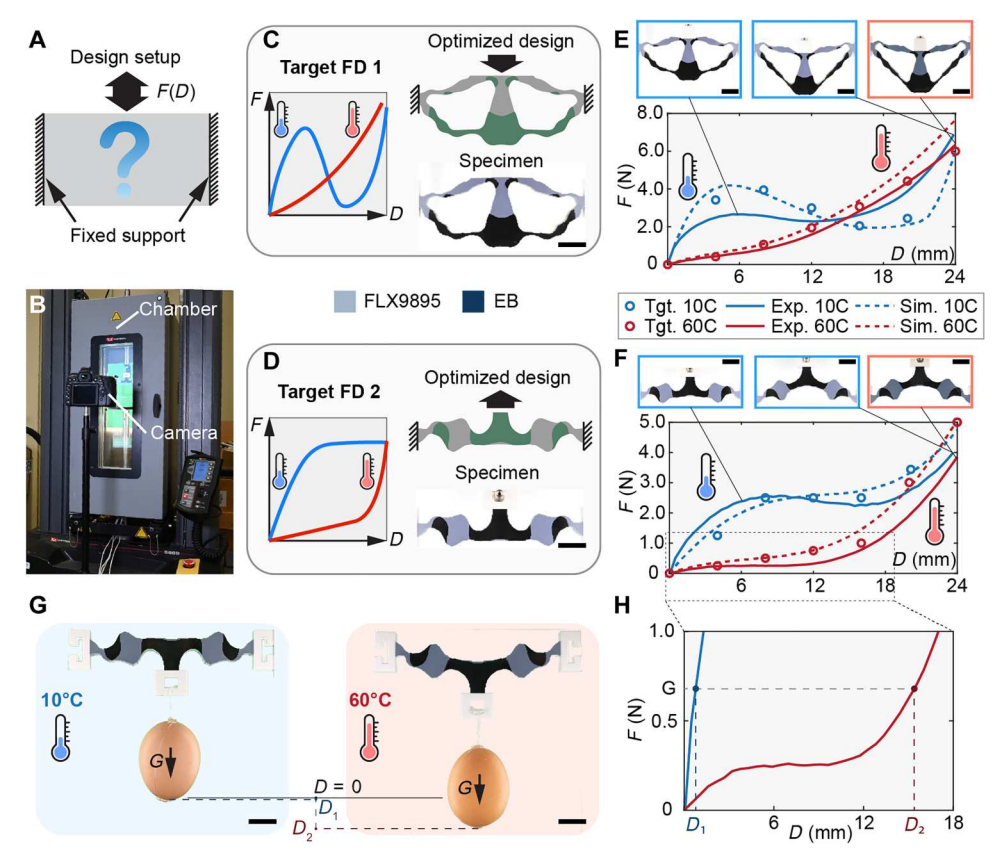


Fig. 2. Realization of programmed adaptive FD responses under different temperatures. (A) Design domain featuring a prescribed vertical displacement at the center and fixed boundaries on both sides. (B) Experimental setup with a thermal chamber. (C and D) Target FD curves and corresponding optimized designs and 3D-printed specimens. The first target features a monotonic stiffening and a metastable buckling response; the second target features a three-stage stiff-plateau-stiff and rapid stiffening behaviors. Scale bars, 20 mm. (E and F) Experimental and simulation FD responses and deformed configurations for targets 1 and 2. Scale bars, 20 mm; (G and H) Demonstration of disparate deformation magnitudes for different temperatures with the same load. See movie S2 for simulation and experimental deformation sequences. Scale bars, 20 mm.

internal connectivity of the unit cell and prevent material failure, we include minimal stiffness constraints in the vertical and lateral directions and a maximum von Mises stress constraint (see section S3.4.2 for details about the formulation). On the basis of this setup, programming dissimilar lateral deformation is realized by specifying different lateral-vertical strain targets under the two temperatures (see section S3.5 for details of the optimization algorithm).

We first focus on metamaterials with an expansion ratio (X strain over Y strain) of -0.4 and 0.6 at 10° and 60° C, respectively. Upon uniaxial loading, the optimized metamaterial (Fig. 3A) would laterally contract at 10° C and expand at 60° C. In the microstructure, FLX occupies most of the design with a small proportion of EB strategically allocated near the center. For validation, the unit cell is assembled in a 3-by-3 pattern (Fig. 3B). To approximate a uniaxial stress state, we allow free lateral displacement at the upper and lower boundaries by using guide rail–roller carriage fixtures (43, 44) between the metamaterials with the loading machine and the thermal chamber (Fig 3B).

The deformed configurations of the metamaterial loaded at 10° and 60°C are shown in Fig. 3 (C and D, respectively), with a zoomed-in view of the center unit cell and its numerical counterpart. The deformed shapes with their reference undeformed

envelopes (dashed box) demonstrate the dissimilar lateral contractions under different temperatures. At 10°C, the contraction is caused mainly by the gradual opening of the two small FLX side branches. The relatively compliant EB, although thicker, cannot restrict the opening of the branches. At 60°C, both materials contribute, and their collective reentrant geometry produces the lateral expansion (auxetic effect). The quantified lateral deformation from the experiment is plotted against the target and simulation in Fig. 4C, demonstrating an accurate realization of the target and a stable expansion ratio over the entire range of applied vertical strain. To further reason the contribution of seemingly superfluous materials, we note that the left- and rightmost small EB parts have a minor but noticeable influence on the metamaterial's overall behavior in that their removal causes a small perturbation to the lateral-vertical strain curves. See section S3.6 for a detailed discussion.

The temperature-dependent deformation can be used for thermal-sensitive switches, as demonstrated in Fig. 3E. Circuits with a blue and a red light-emitting diode (LED) are threaded through the metamaterial with a parallel switch attached to the metamaterial. The circuit is open when the metamaterial is in the rest configuration. When vertically displaced at 10°C, the metamaterial contracts by a predictable distance and closes the blue LED

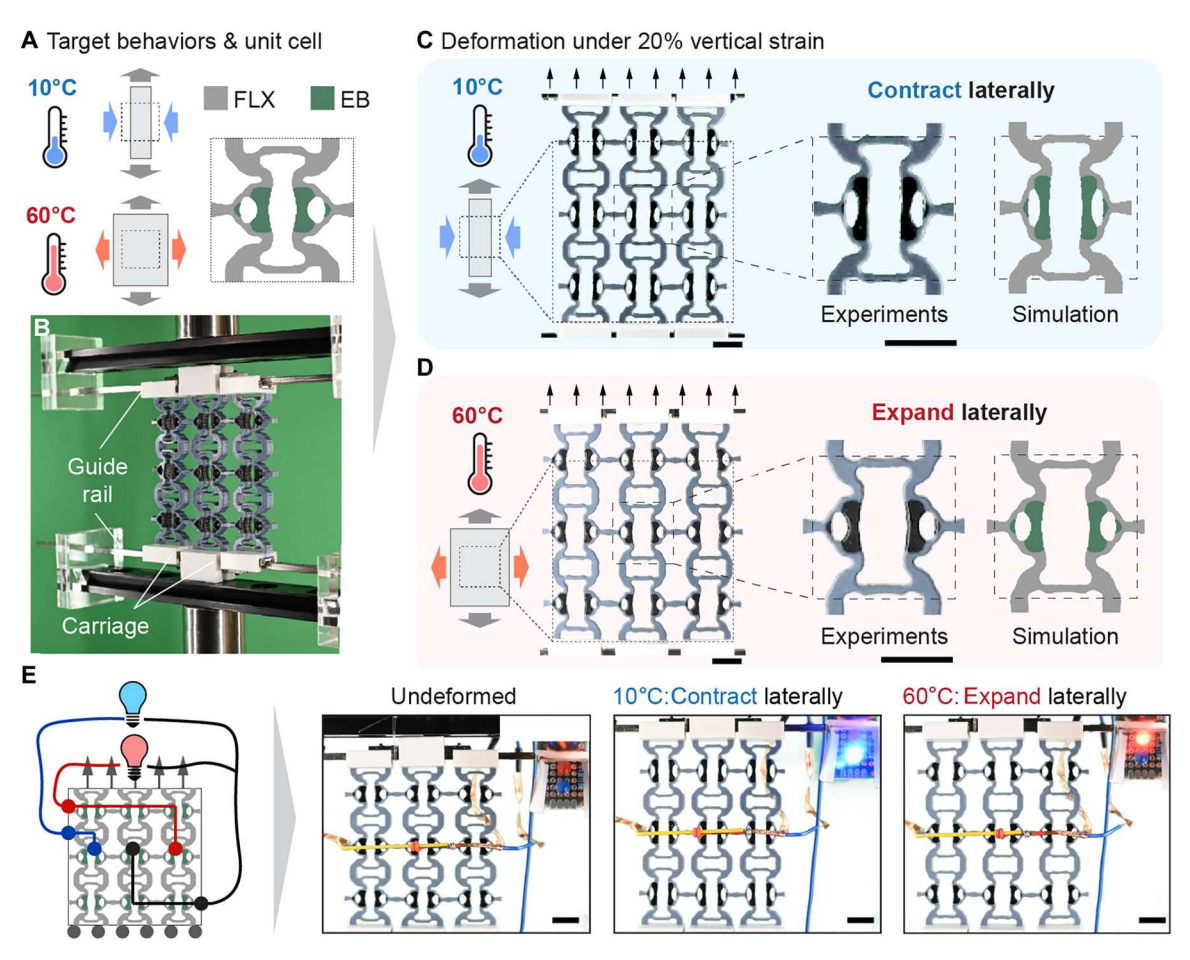


Fig. 3. Realization of temperature-switchable deformation modes with reversed signs under large deformations. (A) Target responses of lateral contraction at 10°C and expansion at 60°C subjected to uniaxial loading and corresponding optimized metamaterial unit cell. (B) Experimental setup for the metamaterial. (C and D) Deformed configurations (experiment) of the metamaterial at 10° and 60°C. Scale bars, 10 mm. (E) Demonstration of a temperature-dependent mechanical switch. Scale bars, 10 mm. See movie S3 for simulation and experimental deformation sequences.

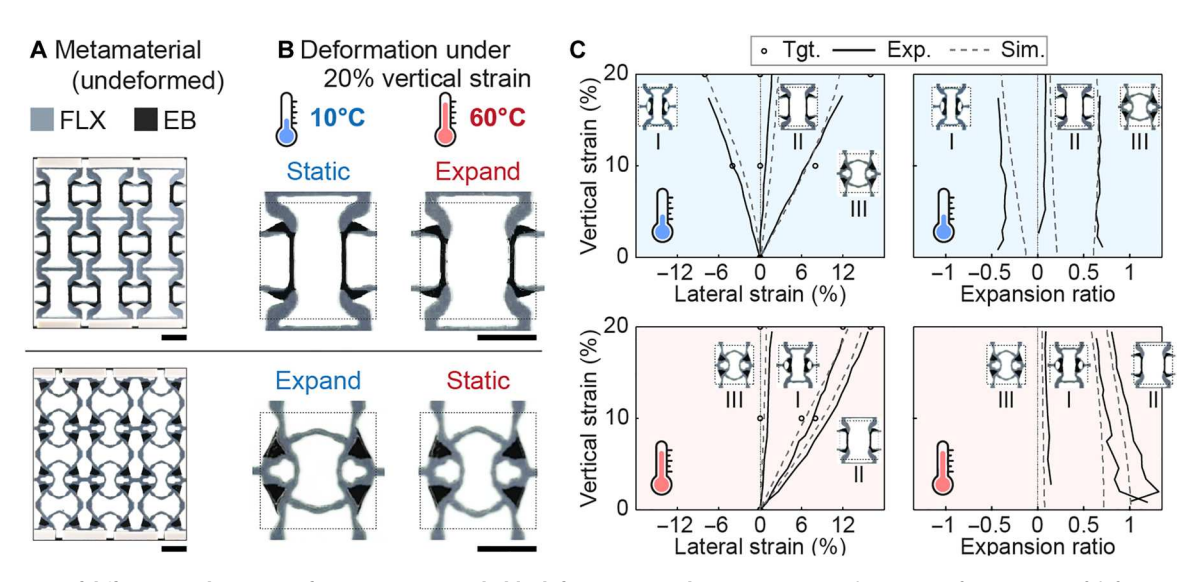


Fig. 4. Realization of different combinations of temperature-switchable deformation modes. (A) Metamaterial specimens for two types of deformation modes: The top one remains laterally static at 10°C and expands at 60°C; the bottom one expands at 10°C and remains static at 60°C. Scale bars, 10 mm. (B) Deformed configurations of metamaterial unit cells at 10° and 60°C. Scale bars, 10 mm. (C) Relations of lateral-vertical average strains and expansion ratio—vertical strain.

circuit. Under 60°C, the metamaterial expands and shifts to close the red LED circuit.

By assigning different target strains in the X (lateral) direction, we can realize different combinations of deformation patterns under the two temperatures. This is demonstrated by the two metamaterials (Dsgs. II and III) in Fig. 4A. Under 10° and 60°C, Dsg. II is programmed to show expansion ratios of 0.0 and 0.8, and Dsg. III would exhibit 0.8 and 0.0 expansion ratios, respectively. The experimental deformed configurations of the unit cells under the two temperatures are shown in Fig. 4B together with the undeformed envelopes. As programmed, Dsg. II has negligible lateral deformation at 10°C and large expansion at 60°C, while Dsg. III expands considerably at 10°C and remains static at 60°C.

The two metamaterials (unit cells) differ fundamentally in geometry and material distributions. Dsg. II has a two-material reentrant geometry mainly consisting of FLX and separated by EB. Hence, at 10°C, the reentrant mechanism is inactive because of the weak spot of EB, and deformation concentrates in the vertical EB members, causing the unit cell to deform only vertically and produce negligible lateral deformation. At 60°C, the reentrant mechanism is activated as both materials contribute and the softened FLX deforms, leading to a large lateral expansion. In contrast to Dsg. II, the reentrant pattern in Dsg. III is formed holistically with FLX and hence is activated at 10°C where FLX dominates. This explains the lateral expansion at 10°C. At 60°C, the thick EB parts retard the reentrant mechanism of the softened FLX parts and inhibit the expansion.

Temperature-switchable and direction-dependent 3D deformation pattern

The giant change in stiffness contrast can be harnessed to realize complex temperature-switchable and direction-dependent 3D deformation patterns. To this end, we use the 3D setup shown in Fig. 5A, where the cubic domain is fixed on a small region at the bottom face and loaded at a small region at the top. We aim to realize expansion in X and contraction in Y at 10°C by a ratio of 0.6 and contraction in X and expansion in Y at 60°C with the same ratio upon being loaded vertically in Z by 15% average strain, as illustrated in Fig. 5A. The regions for the displacement programming are on the side faces of the domain, as indicated by Rgn.1 and Rgn.2 in Fig. 5A. Because of the high computational cost of the 3D setup with full nonlinearity, the optimization requires advanced computational techniques, including a multigrid preconditioned generalized minimal residual linear solver (45-47). Details of the 3D computation and optimization are provided in sections S3.3 and S3.4.3, respectively.

The optimized design and 3D-printed specimen are shown in Fig. 5B, featuring intricately connected members and irregular material distributions, and the final experimental deformation (top view) under the two temperatures are shown in Fig. 5C together with the dashed-line undeformed envelope. The structure exhibits the designed expansion in X and contraction in Y at 10°C and contraction in X and expansion in Y at 60°C. The quantitative experimental displacements are plotted in Fig. 5D with the targets and simulations, demonstrating the accurate achievement of the specified behaviors.

The exotic behavior is a result of the complex geometry and material distribution. The structure has a ring-like component in the mid-height horizontal plane linking Rgn.1 and Rgn.2, and the ring

is connected to the loading region (and support) through several inclined branches. A large portion of the branches connecting Rgn.1 and the loading area is made of EB, while those linking Rgn.2 are completely made of FLX. Hence, when loaded at 10°C, all the inclined branches extend and squeeze the ring member, but because the Rgn.1 branches are much softer than the Rgn.2 branches because of the presence of EB, the Rgn.2 branches dominate and squeeze the ring member to extend in *X* and contract in *Y*. At 60°C, the sharp drop in FLX stiffness makes EB's relative role prominent. When loaded, the squeezing force from the Rgn.1 branches containing EB becomes larger than that from the Rgn.2 branches because, although EB is still softer, its cross section is much thicker than that of the Rgn.2 branches near the loading area. Hence, Rgn.1 contracts and Rgn.2 extends. While this mechanism seems qualitative, the quantitatively accurate fitting requires optimized shapes, sizes, and orientations of all the members, which is realizable only through an inverse design approach.

The temperature-switchable 3D deformation can be used to realize a temperature-dependent electric switch, as demonstrated in Fig. 5E. Serving as the switch, the structure is connected to two different circuits with different light bulbs in the *X* and *Y* directions. The mechanical loading can be seen as a user input of turning on the device. As shown in Fig. 5E, loading the structure at 10°C turns on the blue lights, and loading at 60°C switches on the red lights.

DISCUSSION

This study demonstrates a systematic inverse design and fabrication strategy for realizing arbitrarily programmable temperature-switchable nonlinear responses for mechanical metamaterials. The basic mechanism is the local change of stiffness as a result of distinct glass transition temperatures for different polymers. Full exploitation of the mechanism is enabled by the design freedom of the multimaterial topology optimization-based inverse programming and fabrication freedom of multimaterial 3D printing. The programmed structures and metamaterials feature irregular geometries and material distributions and accurately achieve a broad range of prescribed temperature-tunable nonlinear behaviors. The underlying mechanism is the temperature-induced shift from the sole dominance of one material to the joint influence of both, which fundamentally alters the FD curves and deformation modes in a fully programmable fashion. By demonstrating temperature-directed control of mechanical behavior, we imbue physical intelligence within the architected material. With the rapid development of smart materials, we present a route to create future programmable matters with unprecedented capabilities.

MATERIALS AND METHODS

Material characterization

Given a new multimaterial 3D printer with a rotating gantry, the stress-strain behaviors of all the relevant materials fabricated in different orientations are obtained under ambient conditions. The glass transition temperature is measured using Dynamic Mechanical Analysis (DMA) to select the two materials (FLX and EB) that we used throughout the study. Detailed temperature-dependent characterizations and mathematical modeling are carried out. See section S1 for details.

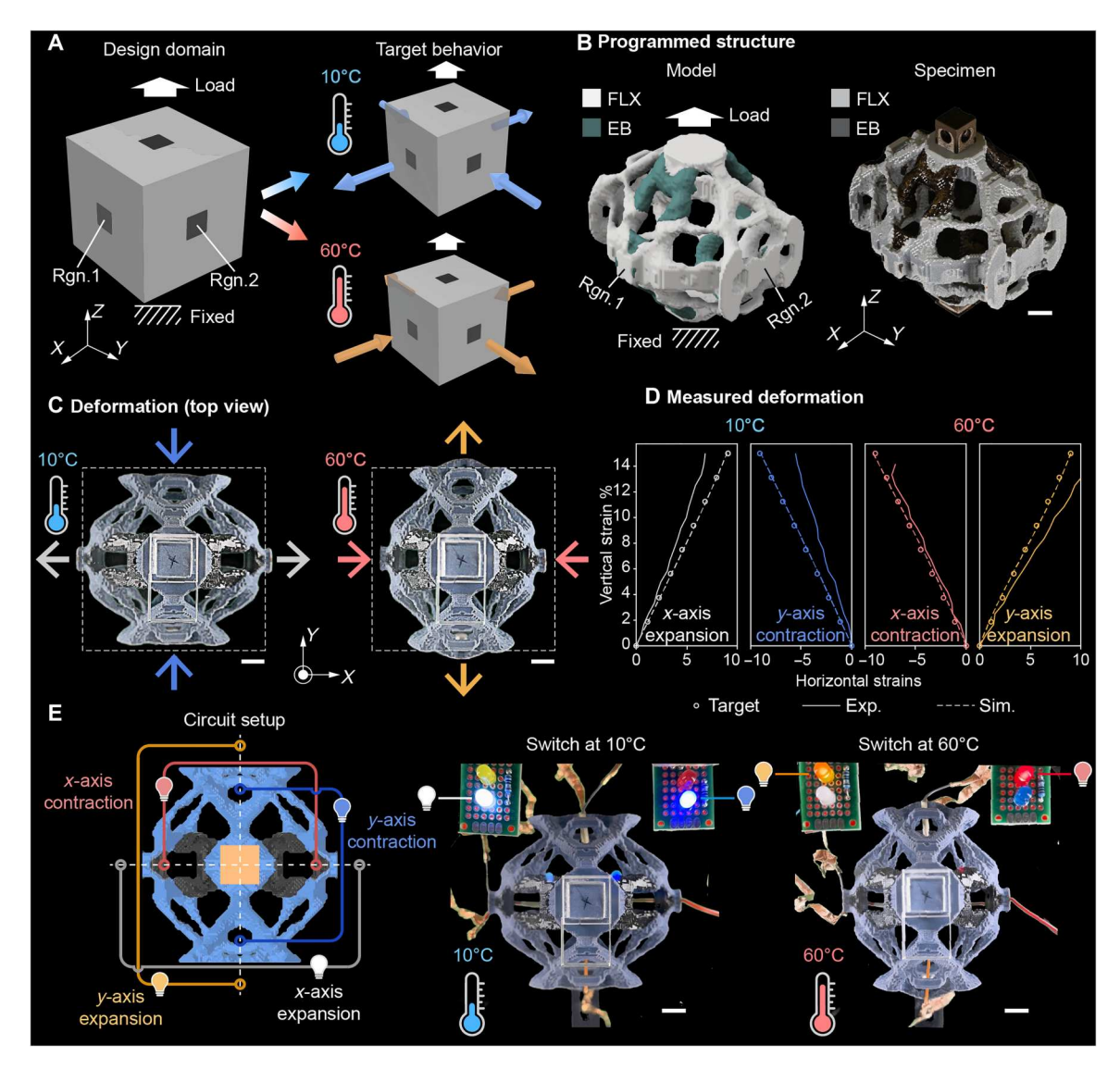


Fig. 5. Temperature-switchable anisotropy for a 3D structure. (A) Design setup and target responses of expansion in X and contraction in Y at 10°C and contraction in X and expansion in Y at 60°C. (B) Optimized design and 3D-printed specimen. Scale bar, 10 mm. (C) Deformed configurations (experiment, top view) of the specimens at 10° and 60°C. Scale bars, 10 mm. (D) Measured lateral displacements at 10° and 60°C. (E) Demonstration of a temperature-dependent 2D switch upon mechanical input in the vertical direction. Scale bars, 10 mm.

Fabrication and experimentation

All specimens in this study are fabricated using a multimaterial PolyJet 3D printer. Mechanical characterizations are performed using a load-testing machine with a temperature chamber. Custom stages are built within the chamber to approximate optimization boundary conditions and to image the deformations. Details can be found in section S2.

Algorithmic generation

Multimaterial topology optimization—based algorithms are used to synthesize all the specimens in this study. While the formulations differ between 2D structures, 2D metamaterials, and 3D structures, all are inverse problems that minimize the errors between finite element predictions and prescribed target responses at multiple displacement points, with different temperatures incorporated as

distinct load cases. Details of the finite element algorithm and optimization formulations are in section S3.

Supplementary Materials

This PDF file includes:

Supplementary Text Figs. S1 to S10

Legends for movies S1 to S3
References

Other Supplementary Material for this manuscript includes the following: Movies S1 to S3

REFERENCES AND NOTES

 T. Toffoli, N. Margolus, Programmable matter: Concepts and realization. Nonli. phenom. 47, 263–272 (1991).

SCIENCE ADVANCES | RESEARCH ARTICLE

- A. Clausen, F. Wang, J. S. Jensen, O. Sigmund, J. A. Lewis, Topology optimized architectures with programmable Poisson's ratio over large deformations. *Adv. Mater.* 27, 5523–5527 (2015).
- J. Panetta, Q. Zhou, L. Malomo, N. Pietroni, P. Cignoni, D. Zorin, Elastic textures for additive fabrication. ACM Trans. Grap. 34, 1–12 (2015).
- K. Bertoldi, V. Vitelli, J. Christensen, M. van Hecke, Flexible mechanical metamaterials. Nat. Rev. Mater. 2, 17066 (2017).
- W. Li, F. Wang, O. Sigmund, X. S. Zhang, Digital synthesis of free-form multimaterial structures for realization of arbitrary programmed mechanical responses. *Proc. Natl. Acad.* Sci. 119, e2120563119 (2022).
- J. Mueller, J. A. Lewis, K. Bertoldi, Architected multimaterial lattices with thermally programmable mechanical response. Adv. Funct. Mater. 32, 2105128 (2022).
- Z. Meng, M. Liu, H. Yan, G. M. Genin, C. Q. Chen, Deployable mechanical metamaterials with multistep programmable transformation. Sci. Adv. 8, eabn5460 (2022).
- H. Yang, N. D'Ambrosio, P. Liu, D. Pasini, L. Ma, Shape memory mechanical metamaterials. Mater. Today 66, 36–49 (2023).
- J. A. Jackson, M. C. Messner, N. A. Dudukovic, W. L. Smith, L. Bekker, B. Moran, A. M. Golobic, A. J. Pascall, E. B. Duoss, K. J. Loh, C. M. Spadaccini, Field responsive mechanical metamaterials. Sci. Adv. 4, eaau6419 (2018).
- Y. Kim, H. Yuk, R. Zhao, S. A. Chester, X. Zhao, Printing ferromagnetic domains for untethered fast-transforming soft materials. *Nature* 558, 274–279 (2018).
- T. Chen, M. Pauly, P. M. Reis, A reprogrammable mechanical metamaterial with stable memory. Nature 589, 386–390 (2021).
- Z. Zhao, X. S. Zhang, Encoding reprogrammable properties into magneto-mechanical materials via topology optimization. npj Comput. Mater. 9, 57 (2023).
- Z. Zhao, C. Wang, X. S. Zhang, Tuning buckling behaviors in magnetically active structures: Topology optimization and experimental validation. J. Appl. Mech. 90, 091006 (2023).
- X. Ning, X. Yu, H. Wang, R. Sun, R. E. Corman, H. Li, C. M. Lee, Y. Xue, A. Chempakasseril, Y. Yao, Z. Zhang, H. Luan, Z. Wang, W. Xia, X. Feng, R. H. Ewoldt, Y. Huang, Y. Zhang, J. A. Rogers, Mechanically active materials in three-dimensional mesostructures. Sci Adv. 4, eaat8313 (2018).
- Y. Wang, L. Li, D. Hofmann, J. E. Andrade, C. Daraio, Structured fabrics with tunable mechanical properties. Nature 596, 238–243 (2021).
- 16. S. Tibbits, 4D printing: Multi-material shape change. Architec. Des. 84, 116–121 (2014).
- X. Kuang, D. J. Roach, J. Wu, C. M. Hamel, Z. Ding, T. Wang, M. L. Dunn, H. J. Qi, Advances in 4D printing: Materials and applications. Adv. Funct. Mater. 29, 1805290 (2019).
- J. M. Rossiter, K. Takashima, F. Scarpa, P. Walters, T. Mukai, Shape memory polymer hexachiral auxetic structures with tunable stiffness. Smart Mater. Struct. 23, 045007 (2014).
- D. Restrepo, N. D. Mankame, P. D. Zavattieri, Programmable materials based on periodic cellular solids. Part i: Experiments. Int. J. Sol. Struct. 100-101, 485–504 (2016).
- M. A. Wagner, T. S. Lumpe, T. Chen, K. Shea, Programmable, active lattice structures: Unifying stretch-dominated and bending-dominated topologies. Extr. Mech. Lett. 29, 100461 (2019).
- C. Yang, M. Boorugu, A. Dopp, J. Ren, R. Martin, D. Han, W. Choi, H. Lee, 4D printing reconfigurable, deployable and mechanically tunable metamaterials. *Mater. Horiz.* 6, 1244–1250 (2019)
- X. Zheng, K. Uto, W.-H. Hu, T.-T. Chen, M. Naito, I. Watanabe, Reprogrammable flexible mechanical metamaterials. Appl. Mater. Today 29, 101662 (2022).
- G. Yao, X. Mo, C. Yin, W. Lou, Q. Wang, S. Huang, L. Mao, S. Chen, K. Zhao, T. Pan, L. Huang, Y. Lin, A programmable and skin temperature–activated electromechanical synergistic dressing for effective wound healing. Sci. Adv. 8, eabl8379 (2022).
- C. Abdol-Hamid Owens, Y. Wang, S. Farzinazar, C. Yang, H. Lee, J. Lee, Tunable thermal transport in 4D printed mechanical metamaterials. *Mater. Des.* 231, 111992 (2023).
- F. Wenz, D. Schönfeld, S. C. L. Fischer, T. Pretsch, C. Eberl, Controlling malleability of metamaterials through programmable memory. Adv. Eng. Mater. 25, 2201022 (2023).
- Z. Meng, W. Qin, T. Mei, C. Qing Chen, Bi-material sinusoidal beam-based temperature responsive multistable metamaterials. Int. J. Sol. Struct. 277-278, 112343 (2023).
- C. Nimmagadda, K. H. Matlack, Thermally tunable band gaps in architected metamaterial structures. J. Sound Vib. 439, 29–42 (2019).
- W. Li, Y. Jia, F. Wang, O. Sigmund, X. S. Zhang, Programming and physical realization of extreme three-dimensional responses of metastructures under large deformations. *Int. J. Eng. Sci.* 191, 103881 (2023).
- K. Guo, Z. Yang, C.-H. Yu, M. J. Buehler, Artificial intelligence and machine learning in design of mechanical materials. *Mater. Horiz.* 8, 1153–1172 (2021).
- M. P. Bendsøe, N. Kikuchi, Generating optimal topologies in structural design using a homogenization method. Comput. Methods Appl. Mech. Eng. 71, 197–224 (1988).
- M. P. Bendsøe, O. Sigmund, Topology Optimization: Theory, Methods and Applications (Springer, 2003).

- X. Zhang, H. Ye, N. Wei, R. Tao, Z. Luo, Design optimization of multifunctional metamaterials with tunable thermal expansion and phononic bandgap. *Mater. Des.* 209, 109990 (2021)
- Stratasys, Digital materials data sheet (2022); www.stratasys.com/siteassets/materials/ materials-catalog/mds_pj_digitalmaterialsdatasheet_0122a-1.pdf?v=49c186.
- J. Mueller, D. Courty, M. Spielhofer, R. Spolenak, K. Shea, Mechanical properties of interfaces in inkjet 3D printed single- and multi-material parts. *Print. Add. Manufact* 4, 193–199 (2017).
- R. Ogden, Elastic deformations of rubberlike solids, in *Mechanics of Solids*, H. Hopkins, M. Sewell, Eds. (Pergamon Press, 1982), pp. 499–537.
- 36. R. W. Ogden, Non-linear Elastic Deformation (Dover Publications, 1997).
- O. Sigmund, S. Torquato, Design of materials with extreme thermal expansion using a three-phase topology optimization method. J. Mech. Phys. Solids 45, 1037–1067 (1997).
- F. Wang, Systematic design of 3D auxetic lattice materials with programmable Poisson's ratio for finite strains. J. Mech. Phys. Solids 114, 303–318 (2018).
- W. Li, F. Wang, O. Sigmund, X. S. Zhang, Design of composite structures with programmable elastic responses under finite deformations. *J. Mech. Phys. Solids* 151, 104356 (2021).
- K. Svanberg, The method of moving asymptotes—A new method for structural optimization. *Int. J. Numer. Methods Eng.* 24, 359–373 (1987).
- S. Shan, S. H. Kang, J. R. Raney, P. Wang, L. Fang, F. Candido, J. A. Lewis, K. Bertoldi, Multistable architected materials for trapping elastic strain energy. *Adv. Mater.* 27, 4296–4301 (2015).
- Q. Zhang, D. Guo, G. Hu, Tailored mechanical metamaterials with programmable quasizero-stiffness features for full-band vibration isolation. *Adv. Funct. Mater.* 31, 2101428 (2021)
- T. Chen, J. Panetta, M. Schnaubelt, M. Pauly, Bistable auxetic surface structures. ACM Trans. Grap. 40, 1–9 (2021).
- K. Liu, P. P. Pratapa, D. Misseroni, T. Tachi, G. H. Paulino, Triclinic metamaterials by tristable origami with reprogrammable frustration. Adv. Mater. 34, e2107998 (2022).
- Y. Saad, M. H. Schultz, Gmres: A generalized minimal residual algorithm for solving nonsymmetric linear systems. SIAM J. Sci. Stat. Comput. 7, 856–869 (1986).
- R. F. Barrett, M. W. Berry, T. F. Chan, J. Demmel, J. M. Donato, J. J. Dongarra, V. Eijkhout, R. Pozo, C. H. Romine, H. A. van der Vorst, *Templates for the Solution of Linear Systems: Building Blocks for Iterative Methods* (Other Titles in Applied Mathematics, SIAM, 1994).
- O. Amir, N. Aage, B. S. Lazarov, On multigrid-cg for efficient topology optimization. Struct. Multidiscp. Optim. 49, 815–829 (2014).
- M. Wagner, T. Chen, K. Shea, Large shape transforming 4D auxetic structures. 3D Print. Addit. Manuf. 4, 133–142 (2017).
- O. Sigmund, Design of multiphysics actuators using topology optimization—Part ii: Twomaterial structures. Comput. Methods Appl. Mech. Eng. 190, 6605–6627 (2001).
- X. S. Zhang, H. Chi, G. H. Paulino, Adaptive multi-material topology optimization with hyperelastic materials under large deformations: A virtual element approach. *Comput. Methods Appl. Mech. Eng.* 370, 112976 (2020).
- F. Wang, B. S. Lazarov, O. Sigmund, J. S. Jensen, Interpolation scheme for fictitious domain techniques and topology optimization of finite strain elastic problems. *Comput. Methods Appl. Mech. Eng.* 276, 453–472 (2014).
- O. Zienkiewicz, R. Taylor, D. Fox, The Finite Element Method for Solid and Structural Mechanics (Butterworth-Heinemann, ed. 7, 2014).
- L. Armijo, Minimization of functions having Lipschitz continuous first partial derivatives. Pacific J. Mathem. 16, 1–3 (1966).
- M. Stolpe, K. Svanberg, On the trajectories of penalization methods for topology optimization. Struct. Multidiscip. Optim. 21, 128–139 (2001).

Acknowledgments

Funding: X.S.Z. and W.L. acknowledge the support by the U.S. NSF CAREER award CMMI-2047692, U.S. NSF EAGER award CMMI-2127134, and U.S. NSF award CMMI-2245251. Y.W. and T. C. acknowledge the support by the U.S. NSF award IIS-2301357. **Author contributions:** Conceptualization: T.C. and X.S.Z. Methodology: W.L., Y.W., T.C., an X.S.Z. Investigation: W.L., Y.W., T.C., and X.S.Z. Supervision: T.C. and X.S.Z. Writing (review and editing): W.L., Y.W., T.C., and X.S.Z. Writing (review and editing): W.L., Y.W., T.C., and X.S.Z. **Competing interests:** The authors declare that they have no competing interests. **Data and materials availability:** All data needed to evaluate the conclusions in the paper are present in the paper and/or the Supplementary Materials.

Submitted 9 August 2023 Accepted 23 October 2023 Published 22 November 2023 10.1126/sciadv.adk0620